scientific reports

Check for updates

OPEN

Impact of the molar activity and PSMA expression level on [^{18}F] AlF-PSMA-11 uptake in prostate cancer

Sarah Piron[1✉], Jeroen Verhoeven[2], Emma De Coster[1], Benedicte Descamps[3], Ken Kersemans[4], Leen Pieters[5], Anne Vral[5], Christian Vanhove[3] & Filip De Vos[1]

This two-part preclinical study aims to evaluate prostate specific membrane antigen (PSMA) as a valuable target for expression-based imaging applications and to determine changes in target binding in function of varying apparent molar activities (MA_{app}) of [^{18}F]AlF-PSMA-11. For the evaluation of PSMA expression levels, male NOD/SCID mice bearing prostate cancer (PCa) xenografts of C4-2 (PSMA+++), 22Rv1 (PSMA+) and PC-3 (PSMA−) were administered [^{18}F]AlF-PSMA-11 with a medium MA_{app} (20.24 ± 3.22 MBq/nmol). SUV_{mean} and SUV_{max} values were respectively 3.22 and 3.17 times higher for the high versus low PSMA expressing tumors ($p < 0.0001$). To evaluate the effect of varying MA_{app}, C4-2 and 22Rv1 xenograft bearing mice underwent additional [^{18}F]AlF-PSMA-11 imaging with a high (211.2 ± 38.9 MBq/nmol) and/or low MA_{app} (1.92 ± 0.27 MBq/nmol). SUV values showed a significantly increasing trend with higher MA_{app}. Significant changes were found for SUV_{mean} and SUV_{max} between the high versus low MA_{app} and medium versus low MA_{app} (both $p < 0.05$), but not between the high versus medium MA_{app} ($p = 0.055$ and 0.25, respectively). The effect of varying MA_{app} was more pronounced in low expressing tumors and PSMA expressing tissues (e.g. salivary glands and kidneys). Overall, administration of a high MA_{app} increases the detection of low expression tumors while also increasing uptake in PSMA expressing tissues, possibly leading to false positive findings. In radioligand therapy, a medium MA_{app} could reduce radiation exposure to dose-limiting organs with only limited effect on radionuclide accumulation in the tumor.

Abbreviations

CT	Computed tomography
IHC	Immunohistochemistry
mCRPC	Metastatic castrate resistant prostate cancer
NAALADase	*N*-Acetylated-α-linked-acidic dipeptidase
OSEM	Ordered subsets maximization expectations
PCa	Prostate cancer
PET	Positron emission tomography
PSMA	Prostate specific membrane antigen
RLT	Radioligand therapy
MA_{app}	Apparent molar activity
SDS-PAGE	Sodium dodecyl sulphate–polyacrylamide gel electrophoresis
SUV	Standardized uptake value
TBoR	Tumor-to-bone ratio
TLR	Tumor-to-liver ratio
TMR	Tumor-to-muscle ratio

[1]Laboratory for Radiopharmacy, Ghent University, Ghent, Belgium. [2]Department of Diagnostic Sciences, Ghent University, Ghent, Belgium. [3]Department of Electronics and Information Systems, IBiTech-MEDISIP, Ghent University, Ghent, Belgium. [4]Department of Medical Imaging, Ghent University Hospital, Ghent, Belgium. [5]Department of Human Structure and Repair, Ghent University, Ghent, Belgium. ✉email: sarah.piron@ugent.be

VOI	Volume of interest
WB	Western blot

Prostate specific membrane antigen (PSMA) is a type II transmembrane glycoprotein that exhibits glutamate carboxypeptidase activity in the proximal small intestines (folate hydrolase) and the brain (NAALADase)[1]. Furthermore, PSMA expression can be found on several tissues including prostate tissue, renal tubules, liver, spleen, and salivary and lacrimal glands[2]. In prostate cancer (PCa) cells, PSMA is expressed 100–1000 fold higher. This overexpression is positively correlated with tumor grade, pathological stage and metastatic castration-resistant prostate cancer (mCRPC), making it an attractive target for both diagnostic and therapeutic purposes[3–5].

For molecular imaging, radiopharmaceuticals are preferably produced with a high molar activity (MA) to ensure that the injected solution contains only a small amount (pico to microgram range) of the tracer substance to avoid pharmacological activity and potential toxic effects. With competitive binding of the radioligand to a target with a saturable receptor density, the chemical mass may affect receptor binding and tracer pharmacokinetics, leading to impaired imaging quality[6]. This mass effect has already been described in the central nervous system, where sub-nanomolar binding affinity ranges and high molar activities are required to distinguish specific from non-specific binding[7,8]. Noguchi et al. demonstrated a positive impact of a high molar activity of [^{11}C] raclopride for characterization of the D_2-receptor in low density regions in the rat brain[9]. For neuroendocrine tumors containing somatostatin receptors, multiple somatostatin-targeting radioligands have shown a dependency between peptide mass and radioligand uptake. Peptide mass-dependent uptake of [^{68}Ga]DOTATOC, a radiolabelled somatostatin receptor ligand, was observed both in organs and tumor tissue[10]. ^{111}In[DOTA^0,TYR^3]octreotide showed an organ-dependent relationship between radioligand uptake and peptide mass, which was suggested to be a balance of the amount of peptide positively influencing receptor clustering while negatively impacting receptor saturation[11]. For [^{111}In]pentreotide, a bell-shaped relationship between specific uptake in octreotide receptor-positive tissues and carrier dose was found. This introduced an additional parameter to ameliorate the target-to-background contrast. Attributing factors to this phenomenon could be receptor accessibility (blood perfusion, presence of endogenous ligand) and receptor binding properties (dissociation constant, rate of internalization and re-expression rate of the receptor)[12]. Furthermore, a simulation study using PBPK modelling investigated the effect of ligand amount, affinity and internalization rate on PSMA imaging and RLT. Overall, the influence of the amount of ligand was more pronounced for radiotracers with a dissociation constant < 1 nM as well as for therapy compared to imaging. Increasing ligand amount significantly reduced absorbed doses in highly perfused or high affinity tissues[13]. These studies show that the amount of peptide administered could be optimized to increase absolute tumor uptake and tumor-to-background ratios.

The impact of the molar activity as a parameter for PET imaging has been investigated for several imaging targets, and it was reported to be highly pronounced for radioligands targeting PSMA. Increasing the amount of peptide had predominantly an effect on uptake in PSMA expressing organs compared to tumors which seemed to be tissue-dependent[14]. Soeda et al. also demonstrated a higher sensitivity of the salivary glands to increasing amounts of peptide compared to tumor tissue using [^{18}F]PSMA-1007, potentially minimizing xerostomia during PSMA radioligand therapy (RLT)[15]. In this two-part preclinical study, we aim to validate PSMA as a target for expression-based imaging by determining the relationship between differences in PSMA expression levels and tumor uptake. Furthermore, changes in the molar activity/amount of peptide of [^{18}F]AlF-PSMA-11 on uptake parameters and tumor-to-organ ratios will be evaluated.

Materials and methods

Synthesis of [^{18}F]AlF-PSMA-11. [^{18}F]AlF-PSMA-11 was synthesized on a modified SynthraFCHOL synthesis module (Synthra GmbH, Hamburg, Germany) as previously reported with some minor modifications[16]. The radiochemical purity was 95.9–97.1% as determined by thin layer chromatography (Alugram RP18-W/UV254 plates (Machery Nagel, Düren, Germany)) using 3:1 v/v acetonitrile in water as mobile phase (Supplementary Fig. 1). Molar activities between 76 and 538 MBq/nmol were achieved as analysed by high performance liquid chromatography (Prevail C18 reversed-phase column, 4.6 × 250 mm, 5 µm, Lokeren, Belgium) and a calibrated dose calibrator (Biodex medical systems, USA) (Supplementary Fig. 2). To achieve differences in apparent molar activity (MA_{app}) levels, varying amounts of a 0.1 µg/µL PSMA-11 (ABX) solution were added to a stock vial to obtain solutions of 1.92 ± 0.27 MBq/nmol (low MA_{app}), 20.06 ± 3.22 MBq/nmol (medium MA_{app}) and 211.2 ± 38.9 MBq/nmol (high MA_{app}).

Preparation of tumor models. The study was approved by the Ghent University Ethical Committee on animal experiments (ECD 18/116). All animals were kept and handled according to the European guidelines (Directive 2010/63/EU). PCa cell lines C4-2 (ATCC; CRL-3314), 22Rv1 (ATCC; CRL-2505) and PC-3 (ATCC; CRL-1435) were cultured using RPMI 1640 medium supplemented with 10% FBS, 1% streptomycin/penicillin (10,000 U/mL) and 1% glutamine 200 mM, and maintained at 37 °C in 5% CO_2 in humidified air. For inoculation, PCa cells were rinsed with FBS-free RPMI 1640 medium and cell suspensions of 5×10^6 cells/100 µL were prepared. Four-to-six-week-old male NOD/SCID mice (Janvier, France) were subcutaneously injected at shoulder height with 200 µL 1:1 cell suspension:Matrigel on either side of each mouse (C4-2, n = 8; 22Rv1, n = 6; PC-3, n = 5). Tumor growth was monitored weekly for 5–6 weeks until tumors reached a diameter between 5 and 10 mm.

Small animal PET/CT imaging. To determine the impact of varying molar activities, each C4-2 xenograft bearing mouse underwent three PET/CT scans within a timeframe of 14 days. On day 1, 7 and 14, mice received either high/low/medium MA_{app} (n = 2) or medium/low/high MA_{app} (n = 4), respectively. The mean adminis-

tered [^{18}F]AlF-PSMA-11 activity was 9.29 ± 0.37 MBq with a mean MA_{app} of either 196.8 ± 32.4 MBq/nmol (high MA_{app}), 19.10 ± 1.69 MBq/nmol (medium MA_{app}) or 1.94 ± 0.274 MBq/nmol (low MA_{app}). To evaluate the activity uptake in PCa tumors with different PSMA expression levels, the images of the medium MA_{app} of C4-2 were compared to PC-3 and 22Rv1. The mean administered activity was 9.30 ± 0.62 MBq [^{18}F]AlF-PSMA-11 with a mean medium MA_{app} of 20.06 ± 3.22 MBq/μg. To evaluate whether the influence of the MA_{app} on low expression tumors, 22Rv1 xenograft bearing mice underwent one additional PET/CT scan on day 7. Each mouse was administered 9.47 ± 0.24 MBq [^{18}F]AlF-PSMA-11 with a high MA_{app} of 243.8 ± 32.8 MBq/nmol.

The images were acquired in list mode using a small animal PET scanner (β-cube, Molecubes, Ghent, Belgium) with a spatial resolution of 0.85 mm and an axial field-of-view of 13 cm. All PET scans were reconstructed into a 192 × 192 × 384 matrix by an ordered subsets maximization expectation (OSEM) algorithm using 30 iterations and a voxel size of 400 × 400 × 400 μm^3.

Immunohistochemical evaluation. After the last scan, two mice/cell line xenograft were sacrificed and tumors were collected for immunohistochemical (IHC) evaluation. Sections were taken from the centre of the tumor sample and stained using Haematoxylin/Eosin, incubated with a primary PSMA antibody (1:400, 2 h, ab133579, Abcam) and counterstained using Haematoxylin (Mayer). Sections were digitally scanned with a virtual scanning microscope (Olympus BX51, Olympus Belgium SA/NV, Berchem, Belgium) at high resolution (20 × magnification).

Western blot analysis. The tumors of the other mice were harvested for western blot (WB) analysis to quantify the PSMA expression levels of the tumor tissues. After thorough rinsing of the tumors, tissue lysates were prepared using RIPA sample buffer. Protein concentrations were determined using the Pierce BCA Protein assay (ThermoFisher Scientific). Samples containing 50 μg of total protein were loaded on 8.5% sodium dodecyl sulphate–polyacrylamide gel electrophoresis (SDS-PAGE) gels. After the transfer, the nitrocellulose membranes were blocked using Odyssey Blocking Buffer (Li-cor Biosciences, Bad Homburg, Germany). Membranes were incubated overnight using a monoclonal PSMA Rabbit anti-Human primary antibody (1:2000, MA533086, Invitrogen, Fischer Scientific, Belgium) and polyclonal Rabbit anti-Human beta actin primary antibody (1:1000, PA1-183, Invitrogen, Fischer Scientific, Belgium), followed by 1 h incubation with IRDye® 800CW Goat anti-Rabbit IgG secondary antibody (1:15,000, Li-cor Biosciences, Bad Homburg, Germany) (Supplementary Fig. 3). The relative densities of both PSMA and β-actin bands were determined using ImageJ[17].

Data analysis. Co-registration and analysis of the PET/CT images was performed using PMOD (PMOD Technologies®, Zürich, Switzerland). Images were visually analysed using the PROMISE criteria. This standardizes image interpretation based on activity uptake in reference tissues (blood, liver and salivary gland) and subdivides suspicious lesions into no, low, intermediate or high PSMA expression[18]. Volumes of interest (VOIs) were drawn manually for delineating the tumor, kidneys, bladder, salivary and lacrimal glands, heart (blood), liver, spleen, muscle and bone. Tissue uptake in each VOI was corrected for residual activity in the syringe and radioactive decay and expressed as SUV_{mean} and SUV_{max}. Furthermore, tumor-to-organ ratios of tissues with a high likelihood for metastases including tumor-to-liver (TLR), tumor-to-muscle (TMR) and tumor-to-bone ratio (TBoR) were determined.

Statistical analysis. All uptake parameters (SUV_{mean}, SUV_{max}, TLR, TMR and TBoR) were reported as mean ± SD. The statistical analysis was performed in R[19] using the Mann–Whitney U test for comparison of uptake between different PSMA expressing xenografts and the Kruskal Wallis test for comparing radioligand uptake of varying MA_{app}, followed by post-hoc pairwise comparison using the Wilcoxon-signed rank test with holm correction for multiple testing. The significance level was set on $p \leq 0.05$.

Ethics approval and consent to participate. The study was approved by the Ghent University Ethical Committee on animal experiments (ECD 18/116). All animals were kept and handled according to the European guidelines (Directive 2010/63/EU). The manuscript complies with the ARRIVE guidelines.

Results

Semi-quantitative analysis of PSMA expression levels in prostate cancer cell lines. The PSMA expression levels were determined by both western blot and immunohistochemical assessment (Fig. 1). WB analysis detected the highest presence of PSMA expression in C4-2 tissue, while only moderate to low expression levels could be observed for 22Rv1. Semi-quantification of blots revealed a β-actin normalized density for PSMA expression of 16.36 ± 3.05 for C4-2 and 0.94 ± 0.21 for 22Rv1 tumors. PC-3 tumors did not show PSMA expression. Similar results were demonstrated by IHC staining, where all C4-2 cells were clearly positively stained for PSMA, while 22Rv1 showed weaker and more heterogeneous staining of the tumor tissue.

Relationship between PSMA expression levels and [^{18}F]AlF-PSMA-11 tumor uptake. Comparative images of [^{18}F]AlF-PSMA-11 uptake (medium MA_{app}) in different PSMA expressing tumors are presented in Fig. 2. Tumor uptake was positively correlated with higher expression levels. According to the PROMISE criteria, PC-3 tumors were PSMA negative (score 0) as tumor uptake was comparable with activity in the blood (heart). 22Rv1 tumors were visually detectable and the tumor activity was higher than the liver and salivary glands, which corresponds to high PSMA expression (score 3). C4-2 tumors showed good image contrast with tumor uptake above activity in the salivary glands (score 3) (Supplementary Table 1).

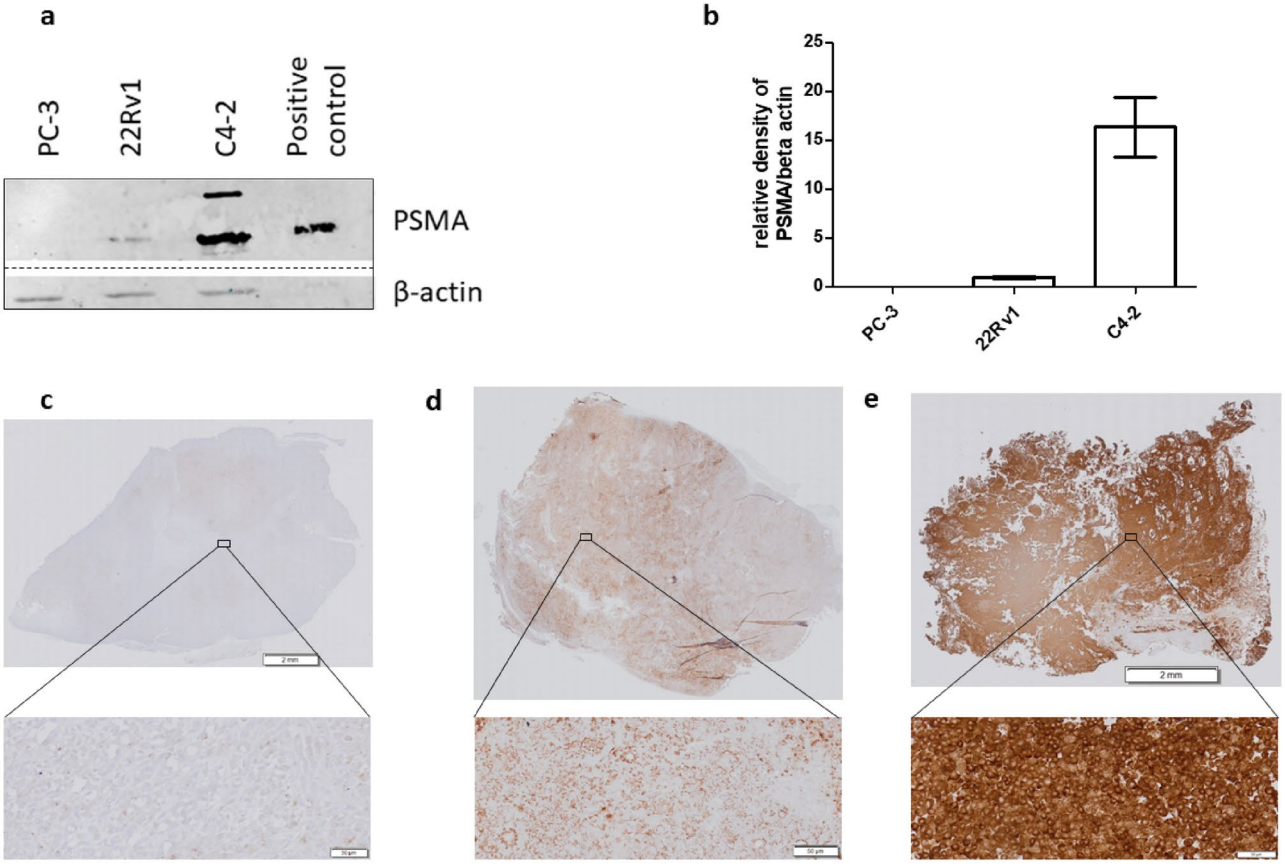

Figure 1. Analysis of PSMA expression levels. WB of PCa tumor tissues and a positive control, all samples were run on the same blot. The non-relevant bands were cropped from the image, the full-length blot is presented in Supplementary Fig. 1 (**a**). Semi-quantification of WB, the relative density of PSMA was normalized using β-actin as loading control. Quantification was only performed using bands from the same blot (**b**). Data for PC-3, 22Rv1 and C4-2 (n = 5) is presented as mean ± SD. IHC of PSMA expression of PC-3 (**c**), 22Rv1 (**d**) and C4-2 (**e**) tumor tissue.

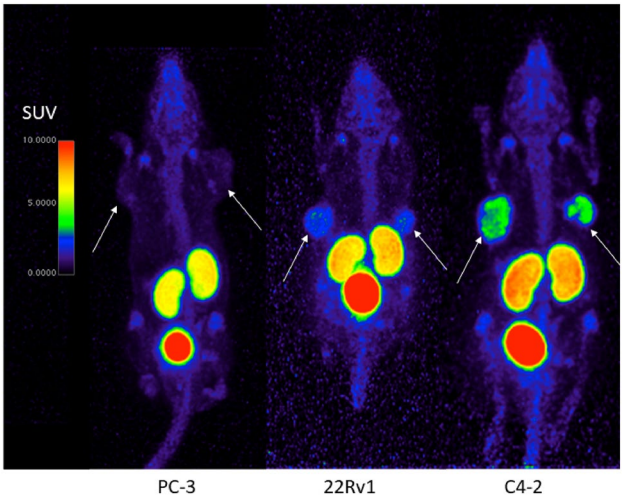

Figure 2. Representative PET images of PC-3 (left), s22Rv1 (middle) and C4-2 (right) xenografts 60 min p.i. of [^{18}F]AlF-PSMA-11 with medium MA_{app}. Arrows indicate tumors. There was no activity uptake detectable in PC-3 tumors, C4-2 and 22Rv1 tumors were visible, although the latter showed less tumor contrast. Color maps were generated using Horos v4.0.0, https://horosproject.org/.

Cell line	Expression level[a]	SUVmean	SUVmax	Tumor-to-liver ratio	Tumor-to-blood ratio[b]	Tumor-to-muscle ratio
PC-3	0	0.09 ± 0.02**	0.22 ± 0.05**	1.38 ± 0.33**	1.41 ± 0.07**	2.26 ± 0.48**
22Rv1	0.94 ± 0.21	0.46 ± 0.11****	1.03 ± 0.23****	6.26 ± 1.41****	6.93 ± 1.49****	6.64 ± 3.81****
C4-2	16.36 ± 3.05	1.48 ± 0.47	3.27 ± 1.07	17.32 ± 3.55	15.47 ± 2.32	19.64 ± 5.37

Table 1. SUV values and tumor-to-organ ratios (liver, blood and muscle) for different PCa tumor cell lines with varying PSMA expression levels: PC-3 (no PSMA expression), 22Rv1 (low PSMA expression) and C4-2 (high PSMA expression). *P* values were calculated using the Wilcoxon signed-rank test with Holm correction with C4-2 as a reference, the significance level was set at $p = 0.05$, $^{**}p < 0.01$, $^{****}p < 0.0001$. [a]Expression levels were determined by semi-quantitative western blot analysis and are expressed β-actin normalized density. [b]Activity in blood was determined by delineation of the heart.

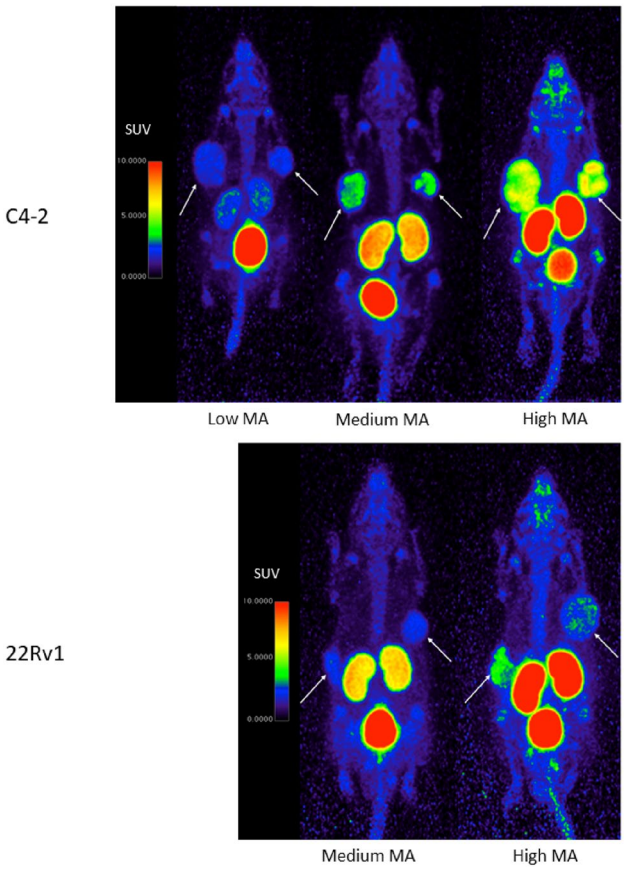

Figure 3. Representative PET images after [^{18}F]AlF-PSMA-11 injection of C4-2 (top) and 22Rv1 (bottom) xenografts of low (only C4-2), medium and high MA_{app} images in the same animal. Arrows indicate tumors. Increasing MA_{app} resulted in higher activity uptake in tumors as well as the kidneys, while activity in the bladder decreased. Color maps were generated using Horos v4.0.0, https://horosproject.org/.

Quantitative VOI analysis demonstrated significant differences for SUV_{mean} and SUV_{max} as well as tumor-to-organ ratios including tumor-to-liver, tumor-to-blood and tumor-to-muscle in function of PSMA expression levels (Table 1). When comparing C4-2 (high PSMA expression) to 22Rv1 (low PSMA expression), SUV_{mean} and SUV_{max} values were approximately 3.22 and 3.17 times higher, respectively ($p < 0.0001$). Similar ratios of 2.77, 2.23 and 2.96 were found for tumor-to-liver, tumor-to-blood and tumor-to-muscle, respectively ($p < 0.0001$). SUV values were significantly lower for PC-3 tumors compared to both C4-2 ($p < 0.01$) and 22Rv1 tumors ($p < 0.001$).

Impact of the molar activity on tumor uptake. To evaluate the impact of the MA_{app} on tumor uptake, all C4-2 xenograft bearing mice underwent three PET/CT scans with different MA_{app} levels (high $MA_{app} = 194.8 \pm 32.1$ MBq/nmol, medium $MA_{app} = 18.91 \pm 1.67$ MBq/nmol and low $MA_{app} = 1.92 \pm 0.27$ MBq/nmol). Images show high uptake in C4-2 tumors after injection of a high MA_{app} activity dose, which decreased with lower MA_{app} (Fig. 3). Kidney uptake decreased as well with lower MA_{app} while activity in de bladder

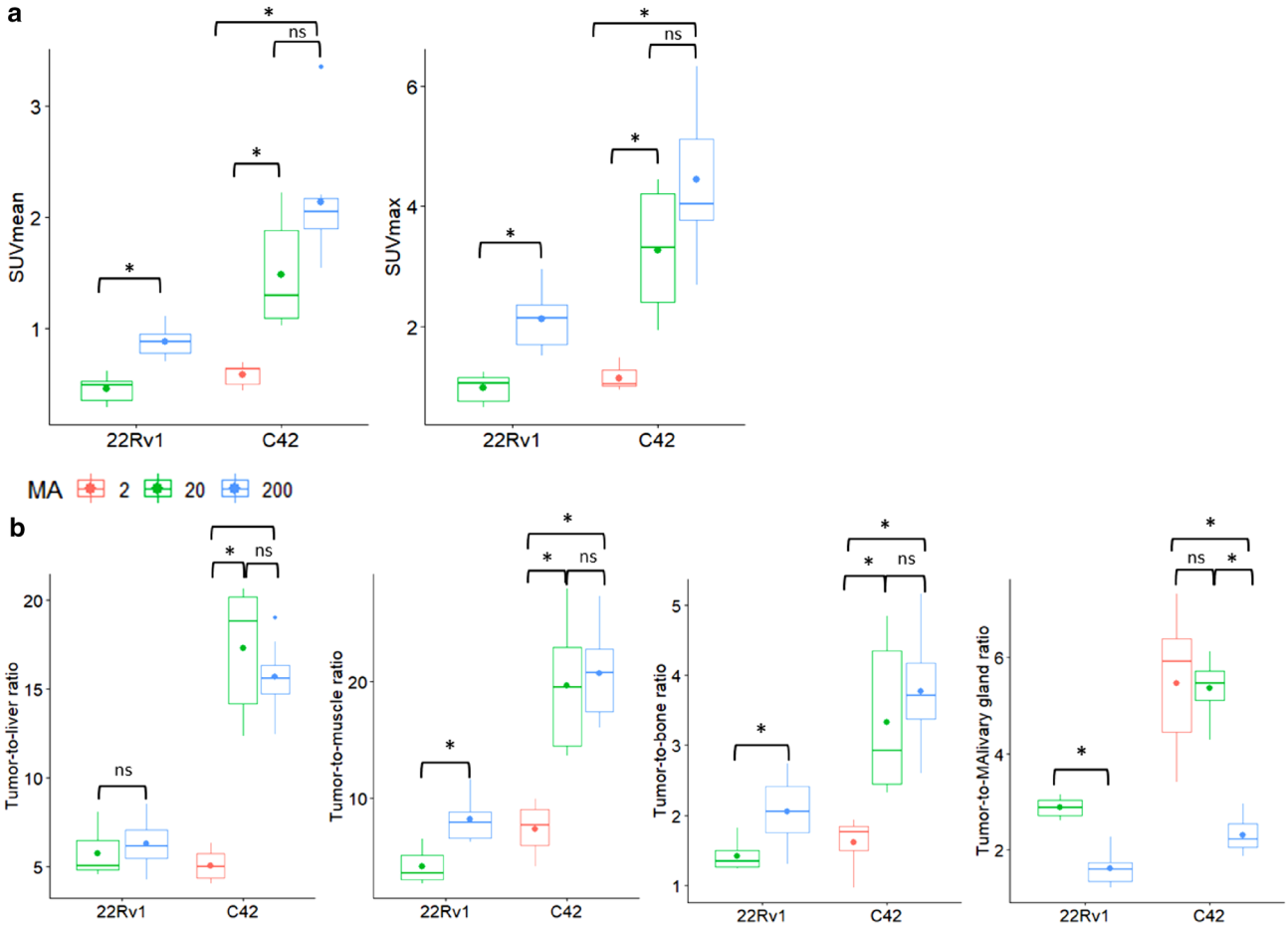

Figure 4. SUV_{mean} (left) and SUV_{max} (right) (**a**) and tumor-to-liver, tumor-to-muscle, tumor-to-bone and tumor-to-salivary gland ratio (**b**) of 22Rv1 and C4-2 tumors after imaging with either the low MA_{app} (0.94 ± 0.27 MBq/µg, only C4-2), medium MA_{app} (20.26 ± 3.25 MBq/µg) or high MA_{app} (213.3 ± 39.3 MBq/µg) [^{18}F]AlF-PSMA-11 60 min p.i.. The mean values were added as dots to the boxplot. The significance level was set at $p = 0.05$. *Ns* = not significant, *$p < 0.05$.

increased. PSMA expressing tissues such as salivary glands, lacrimal glands and spleen were clearly visible on high MA_{app} PET images but were barely visible on medium MA_{app} images and not detectable on low MA_{app} images (Supplementary Table 2).

When comparing intra-individual tumor uptake of the high, medium and low MA_{app}, SUV_{mean} (2.14 ± 0.54, 1.48 ± 0.47 and 0.58 ± 0.10, respectively) and SUV_{max} (4.44 ± 1.25, 3.27 ± 1.07 and 1.15 ± 0.19, respectively) showed a significantly decreasing trend (both $p < 0.001$). Post-hoc pairwise comparison revealed statistically significant changes between the high and low MA_{app} ($p < 0.05$) as well as between the medium and low MA_{app} ($p < 0.05$), but not between the high and medium MA_{app} ($p = 0.055$ and 0.25, respectively) (Fig. 4a). Additionally, 22Rv1 xenograft bearing mice (n = 3) received an additional PET/CT scan with high MA_{app} (246.3 ± 33.1 MBq/µg). Comparison of SUV_{mean} and SUV_{max} values demonstrated a statistically significant difference between the high and medium MA_{app} (both $p = 0.031$).

Tumor-to-organ ratios were determined for tissues with a high likelihood for metastases including liver (TLR), muscle (lymph nodes) (TMR) and bone (TBoR). In C4-2 xenografts, tumor-to-organ ratios remained constant between the high and medium MA_{app} for TLR (15.71 ± 1.99 vs 17.32 ± 3.55, $p = 0.46$), TMR (20.69 ± 3.82 vs 19.64 ± 5.37, $p = 0.74$) and TBoR (3.77 ± 0.78 vs 3.33 ± 1.03, $p = 0.31$) while a statistically significant difference could be observed for high versus low MA_{app} and medium versus low MA_{app} (Fig. 4b). A similar trend between the high and medium MA_{app} was found for 22Rv1 xenografts, however, the tumor-to-liver ratio remained constant. On the other hand, SUV_{mean} values of PSMA expressing tissues such as salivary and lacrimal glands, spleen, and kidneys significantly decreased between the high and medium MA_{app} ($p < 0.01$) (Fig. 5). Tumor-to-salivary gland ratios increased from 2.30 ± 0.37 for the high MA_{app} to 5.35 ± 0.59 for the medium MA_{app}. While kidney uptake significantly decreased, uptake in the bladder rose for the medium and low MA_{app}.

Discussion

Although the diagnostic applications of PSMA as a target for imaging have been the subject of many clinical trials, preclinical studies are essential for a comprehensive investigation of several important aspects of PSMA PET imaging. In this paper, [^{18}F]AlF-PSMA-11 was used for imaging experiments to further understand PSMA

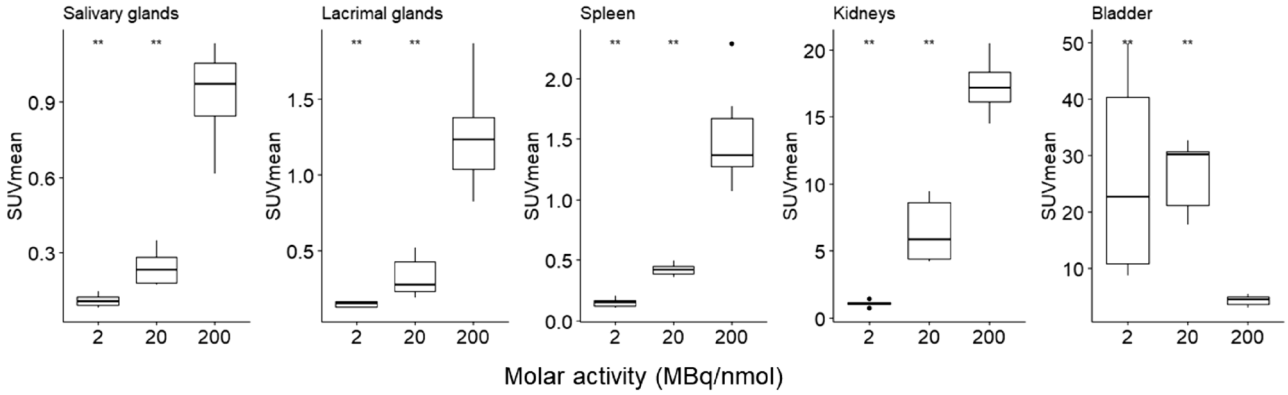

Figure 5. C4-2 xenograft bearing mice were injected with [^{18}F]AlF-PSMA-11 with either a low MA_{app} (1.92 ± 0.27 MBq/µg), medium MA_{app} (18.91 ± 1.67 MBq/µg) or high MA_{app} (194.8 ± 32.1 MBq/µg). Boxplots represent SUV_{mean} values 60 min p.i. of PSMA expressing tissues including salivary glands, lacrimal glands, spleen and excretory organs (kidneys and bladder). The high MA_{app} was set as reference and the significance level was set at $p = 0.05$. *Ns* = not significant, $^{**}p < 0.01$.

PET imaging. First, PSMA was validated as a valuable target for expression-based applications by determining the relationship between PSMA expression levels and [^{18}F]AlF-PSMA-11 tumor uptake. This was examined using three human PCa cell lines with high (C4-2), low (22Rv1) and no detectable (PC-3) PSMA expression. Second, changes in target binding of PSMA positive tumors and tissues using varying amounts of cold PSMA-11 peptide were evaluated.

The relationship between target expression levels and [^{18}F]AlF-PSMA-11 uptake was determined by PET/CT imaging of mice bearing PCa tumors with varying PSMA expression levels. The use of a medium MA_{app} for the expression level experiments was selected based on several practical considerations. A larger group of mice could be imaged on the same day, while the use of the high MA_{app} would significantly limit the size of the study population. Also, using the high MA_{app} would introduce a larger variation in the MA_{app} between animals, as the amount of PSMA-11 precursor is so small, that minor differences in amount of precursor added to the stock solution would lead to large differences in MA_{app}. Semi-quantitative western blot analysis showed that PSMA expression levels of C4-2 tumors were approximately 16 times higher compared to 22Rv1 tumors, while SUV values were only 3 times higher. A positive association between PSMA expression and SUV values could be found. Although 22Rv1 tumors had only low PSMA expression levels on western blot, activity uptake was above the liver, scoring positively (score 3) according to the PROMISE criteria. This suggests the ability of [^{18}F]AlF-PSMA-11 to detect PCa lesions, even with low PSMA receptor abundancy. Increasing the MA_{app} of [^{18}F]AlF-PSMA-11 increased absolute SUV_{mean} and SUV_{max} values (Fig. 4), but due to higher salivary gland uptake, the PROMISE score did not increase. However, TMR and TBoR did increase significantly, which could be beneficial for the detection of lymph nodes and bone metastases with low PSMA expression levels, although this should be confirmed in a murine model of bone metastases. Lückerath et al. determined the in vivo correlation between [^{68}Ga]PSMA-11 PET/CT and PSMA expression using four murine PCa cell lines. [^{68}Ga]PSMA-11 PET was able to detect changes in PSMA expression at low levels, but this sensitivity was lost at higher PSMA levels, which is in agreement with the reported non-linear correlation[20].

PSMA expression was shown to be an important prognosticator for overall survival of metastatic castrate resistant prostate cancer (mCRPC) patients under [^{177}Lu]PSMA treatment. The presence of low average-PSMA expressing tumors was found to be a negative prognostic factor in these patients[21]. The threshold for determining the PSMA expression level was based on the criterium set by Hofman et al. who defined high PSMA expression as any metastatic lesion with a SUV_{max} of 1.5 times the liver SUV. Here, [^{177}Lu]PSMA therapy resulted in 50% decline in PSA for 17/30 mCRPC patients presenting with high PSMA expression metastases[22]. The liver seems to be a solid choice as reference organ as our results show that changes in the MA_{app} did not significantly alter tumor-to-liver ratios (between the high and medium MA_{app}). It should however be noted that the difference in chemical structure between [^{177}Lu]PSMA-617 and [^{18}F]AlF-PSMA-11 could also have an influence on biodistribution and clearance pathways. Additional research should determine to which extent PSMA expression levels could be used as an exclusion criterium for [^{177}Lu]PSMA therapy. In our study, the difference between the medium and high MA_{app} was more pronounced in low expression 22Rv1 tumors. SUV values, TMR and TBoR increased significantly when administering the high MA_{app}. This can be attributed to the lower amount of receptors available to bind radiolabelled PSMA molecules and more rapid saturation in the presence of a larger peptide mass.

Overall, the highest mean absolute SUV_{mean} and SUV_{max} values were obtained after administration of [^{18}F]AlF-PSMA-11 with high MA_{app}, but the difference between the medium and high MA_{app} was not statistically significant, both for SUV values as for tumor-to-organ ratios (TLR, TMR and TBoR). There was however a substantial decrease of activity uptake in PSMA expressing tissues (salivary and lacrimal glands, spleen and kidneys) between the high and medium MA_{app}. The use of medium MA_{app} [^{18}F]AlF-PSMA-11 could therefore reduce activity uptake in PSMA positive healthy tissues while maintaining image contrast of tumor metastases compared to the surrounding tissue. This would be beneficial for both diagnostic purposes and radioligand therapy. Prostate cancer lesions could be more reliably detected due to the constant tumor-to-organ ratio while

less non-specific uptake could facilitate scan interpretation by limiting the potential pitfalls of PSMA PET caused by aspecific physiological uptake[23]. In radioligand therapy, healthy tissue would be less exposed to the radiation while absolute tumor uptake would remain approximately constant.

During PSMA radioligand therapy, radiation exposure caused by activity uptake in PSMA-expressing non-tumor tissues can cause dose-limiting toxic side effects. Radioligand uptake in the salivary glands causes xerostomia and can be a reason for treatment discontinuation[24,25]. Lowering the MA_{app} for RLT ligands could be a useful tool for reducing radiation exposure and should be further investigated as an alternative for botulinum toxin injections[26] or sialendoscopy and dilatation combination with saline irrigation and steroid injections[27]. A preclinical study by Fendler et al. also showed that administration of [^{177}Lu]PSMA-617 with a molar activity of 62 MBq/nmol achieved the highest tumor-to-salivary gland ratio compared to lower molar activities (31 and 15 MBq/nmol)[28]. When correcting for the administered dose of 60 MBq, the highest molar activity corresponds to 0.97 nmol PSMA-617, which is in the same range as our medium MA_{app} group (0.49 nmol PSMA-11) that also showed the highest tumor-to-salivary gland ratio. However, it was reported that the low to moderate PSMA staining on IHC staining does not correlate with the high PSMA radioligand accumulation. It was hypothesized that tracer accumulation in the salivary glands is therefore a combination of both specific and non-specific uptake[29]. The latter mechanism is not yet elucidated and our results show a large impact of a higher amount of peptide on activity uptake in salivary glands, suggesting that this as a promising direction for further research. The difference in PSMA expression between murine and human salivary glands must also be taken into consideration. As the binding affinity and PSMA concentration in murine salivary glands is lower compared to human salivary glands, it would be expected that the influence of molar activities will be more pronounced in humans[30]. Another organ-at-risk are the kidneys. Renal clearance can lead to accumulation of radiolabelled peptides in the tubular cells where it irradiates the kidneys, potentially leading to renal dysfunction, particularly in patients with a known history of nephropathy. Although no major nephrotoxicity was reported for [^{177}Lu]PSMA[31], chronic kidney disease was reported in two patients for [^{225}Ac]PSMA therapy. Limiting kidney exposure to [^{255}Ac]PSMA may decrease toxicity and maintain its therapeutic potential[32]. A study by Kratochwil et al. investigated the influence of additional 2-PMPA administration on tumor and kidney uptake using [^{125}I]MIP-1095. Injection of low doses 2-PMPA (0.2–1 mg/kg) 16 h after tracer administration significantly increased the tumor-to-kidney ratio[33]. These results indicate potential benefits of the use of cold precursor or PSMA inhibitory small molecules such as 2-PMPA for reducing radiation exposure to the kidneys. Additionally, a high tumor load in patients can also lead to reduced activity uptake in dose-limiting organs[34]. [^{18}F]AlF-PSMA-11 might therefore be applied as a diagnostic tool for individual optimization of RLT protocols considering PET-based tumor load and radioligand MA_{app}.

These results show the importance of the amount of carrier on tumor targeting strategies. The optimal amount should be low to avoid competitive binding of unlabelled molecules at the target site but not too low as the tracer molecules could be trapped in non-specific binding places. For diagnostic purposed, using a high MA_{app} will increase the detection of low expression tumors while also increasing specific uptake in PSMA expressing tissues, possibly leading to false positive findings. For radioligand therapy, further research should focus on finding a balance between administration of a high MA_{app} for high absolute uptake in the tumor tissue while minimizing activity uptake in healthy organs in order to reduce dose-limiting toxicity. Also, although the considerations mentioned before are valid for high PSMA expressing PCa lesions, decreasing the MA_{app} to limit non-specific uptake could also affect the detectability of low PSMA expressing lesions, which could lead to an underestimation of the tumor burden.

A major limitation of this study is the translation from mouse to human. Although the differences in the administered MA_{app} in mice gave well defined results, the activity dose and amount of peptide that is administered compared to total body weight for PET/CT is different for mice and humans, which makes translation into clinical applications more challenging. However, as the molar activity of a PSMA PET tracer decreases over time, it would be beneficial to evaluate the effect on both tumor uptake and non-target uptake in humans. In a retrospective analysis of patients who underwent [^{18}F]rhPSMA-7.3 PET/CT, only minor effects on biodistribution were found for a tenfold decrease of MA_{app}, except for the salivary glands and spleen, which showed significantly lower uptake for the lower molar activity[35]. Overall, these results encourage a prospective clinical trial using [^{18}F]AlF-PSMA-11 comparing a high to medium MA_{app}.

Due to the intra-individual comparison of MA_{app} levels, most mice were imaged multiple times and tumor sizes differed slightly between scans. However, the tumor size was many times higher than the PET resolution and mice were randomized for MA_{app} sequence, therefore minimizing this limitation as much as possible.

Conclusion

This paper evaluated [^{18}F]AlF-PSMA-11 PET for expression-based imaging of prostate cancer and the effect of the amount of carrier administered on tumor uptake and tumor-to-organ ratios. A positive association was found between PSMA expression and tumor uptake. The highest absolute tumor uptake was obtained by the high MA_{app}. And although activity uptake in PSMA expressing organs decreased significantly with lower MA_{app}, there was no statistically significant difference in tumor SUV between the high and medium MA_{app}. These results suggest that administration of a high MA_{app} increases the detection of low expression tumors while also increasing specific uptake in PSMA expressing tissues, possibly leading to false positive findings. In radioligand therapy, a medium MA_{app} could reduce radiation exposure to dose-limiting organs with only limited effect on radionuclide accumulation in the tumor. Overall, it is of utmost importance to validate the association between both PSMA expression and molar activity relative to radioligand activity uptake.

Data availability

The datasets and images used and/or analysed during the current study are available from the corresponding author on reasonable request.

Received: 17 September 2021; Accepted: 10 November 2021
Published online: 19 November 2021

References

1. Barinka, C., Rojas, C., Slusher, B. & Pomper, M. Glutamate carboxypeptidase II in diagnosis and treatment of neurologic disorders and prostate cancer. *Curr. Med. Chem.* **19**(6), 856–870 (2012).
2. Silver, D. A., Pellicer, I., Fair, W. R., Heston, W. D. W. & Cordon-Cardo, C. Prostate-specific membrane antigen expression in normal and malignant human tissues'. *Clin. Cancer Res.* **3**(81), 81–85 (1997).
3. Bostwick, D. G., Pacelli, A., Blute, M., Roche, P. & Murphy, G. P. Prostate specific membrane antigen expression in prostatic intraepithelial neoplasia and adenocarcinoma: A study of 184 cases. *Cancer* **82**(11), 2256–2261 (1998).
4. Ross, J. S. *et al.* Correlation of primary tumor prostate-specific membrane antigen expression with disease recurrence in prostate cancer. *Clin. Cancer Res.* **9**(17), 6357–6362 (2003).
5. Bravaccini, S. *et al.* PSMA expression: A potential ally for the pathologist in prostate cancer diagnosis. *Sci. Rep.* **8**(1), 4254 (2018).
6. Kung, M. P. & Kung, H. F. Mass effect of injected dose in small rodent imaging by SPECT and PET. In *Nuclear Medicine and Biology*, vol. 32, 673–678. (Elsevier Inc., 2005).
7. Nebel, N., Maschauer, S., Kuwert, T., Hocke, C. & Prante, O. In vitro and in vivo characterization of selected fluorine-18 labeled radioligands for PET imaging of the dopamine D3 receptor. *Molecules* **21**(9), 1144 (2016).
8. Javed, M. R. *et al.* High yield and high specific activity synthesis of [^{18}F]fallypride in a batch microfluidic reactor for micro-PET imaging. *Chem. Commun.* **50**(10), 1192–1194 (2014).
9. Noguchi, J., Zhang, M. R., Yanamoto, K., Nakao, R. & Suzuki, K. In vitro binding of [^{11}C]raclopride with ultrahigh specific activity in rat brain determined by homogenate assay and autoradiography. *Nucl. Med. Biol.* **35**(1), 19–27 (2008).
10. Velikyan, I. *et al.* In vivo binding of [^{68}Ga]-DOTATOC to somatostatin receptors in neuroendocrine tumours—Impact of peptide mass. *Nucl. Med. Biol.* **37**(3), 265–275 (2010).
11. De Jong, M. *et al.* Tumour uptake of the radiolabelled somatostatin analogue [DOTA0, TYR3]octreotide is dependent on the peptide amount. *Eur. J. Nucl. Med.* **26**(7), 693–698 (1999).
12. Breeman, W. A. P. *et al.* Effect of dose and specific activity on tissue distribution of indium-111-pentetreotide in rats. *J. Nucl. Med.* **36**(4), 623LP-627LP (1995).
13. Begum, N. J. *et al.* The effect of ligand amount, affinity and internalization on PSMA-targeted imaging and therapy: A simulation study using a PBPK model. *Sci. Rep.* **9**(1), 1–8 (2019).
14. Wurzer, A. *et al.* Molar activity of Ga-68 labeled PSMA inhibitor conjugates determines PET imaging results. *Mol. Pharm.* **15**(9), 4296–4302 (2018).
15. Soeda, F. *et al.* Impact of 18F-PSMA-1007 uptake in prostate cancer using different peptide concentrations: Preclinical PET/CT study on mice. *J. Nucl. Med.* **60**(11), 1594–1599 (2019).
16. Kersemans, K. *et al.* Automated radiosynthesis of Al[^{18}F]PSMA-11 for large scale routine use. *Appl. Radiat. Isot.* **135**, 19–27 (2018).
17. Schneider, C. A., Rasband, W. S. & Eliceiri, K. W. NIH image to ImageJ: 25 years of image analysis. In *Nature Methods*, vol. 9, 671–675. (Nature Publishing Group, 2012).
18. Eiber, M. *et al.* Prostate cancer molecular imaging standardized evaluation (PROMISE): Proposed miTNM classification for the interpretation of PSMA-ligand PET/CT. *J. Nucl. Med.* **59**(3), 469–478 (2018).
19. R Core Team. *R: A Language and Environment for Statistical Computing* (R Foundation for Statistical Computing, 2019).
20. Lückerath, K. *et al.* Detection threshold and reproducibility of ^{68}Ga-PSMA11 PET/CT in a mouse model of prostate cancer. *J. Nucl. Med.* **59**(9), 1392–1397 (2018).
21. Seifert, R. *et al.* Analysis of PSMA expression and outcome in patients with advanced prostate cancer receiving ^{177}Lu-PSMA-617 radioligand therapy. *Theranostics* **10**(17), 7812–7820 (2020).
22. Hofman, M. S. *et al.* [^{177}Lu]-PSMA-617 radionuclide treatment in patients with metastatic castration-resistant prostate cancer (LuPSMA trial): A single-centre, single-arm, phase 2 study. *Lancet Oncol.* **19**(6), 825–833 (2018).
23. Mei, R., Farolfi, A., Castellucci, P., Nanni, C., Zanoni, L. & Fanti, S. PET/CT variants and pitfalls in prostate cancer: What you might see on PET and should never forget. *Semin. Nucl. Med.* **51**, 621–632 (2021).
24. Kratochwil, C. *et al.* Targeted a-therapy of metastatic castration-resistant prostate cancer with ^{225}Ac-PSMA-617: Swimmer-plot analysis suggests efficacy regarding duration of tumor control. *J. Nucl. Med.* **59**(5), 795–802 (2018).
25. Langbein, T., Chaussé, G. & Baum, R. P. Salivary gland toxicity of PSMA radioligand therapy: Relevance and preventive strategies. *J. Nucl. Med.* **59**(8), 1172–1173 (2018).
26. Baum, R. P. *et al.* Injection of botulinum toxin for preventing salivary gland toxicity after PSMA radioligand therapy: An empirical proof of a promising concept. *Nucl. Med. Mol. Imaging* **52**(1), 80–81 (2018).
27. Rathke, H. *et al.* Initial clinical experience performing sialendoscopy for salivary gland protection in patients undergoing ^{225}Ac-PSMA-617 RLT. *Eur. J. Nucl. Med. Mol. Imaging* **46**(1), 139–147 (2019).
28. Fendler, W. P. *et al.* Establishing ^{177}Lu-PSMA-617 radioligand therapy in a syngeneic model of murine prostate cancer. *J. Nucl. Med.* **58**(11), 1786–1792 (2017).
29. Rupp, N. J. *et al.* First clinicopathologic evidence of a non-PSMA-related uptake mechanism for ^{68}Ga-PSMA-11 in salivary glands. *J. Nucl. Med.* **60**(9), 1270–1276 (2019).
30. Roy, J. *et al.* Comparison of prostate-specific membrane antigen expression levels in human salivary glands to non-human primates and rodents. *Cancer Biother. Radiopharm.* **35**(4), 284–291 (2020).
31. Gallyamov, M., Meyrick, D., Barley, J. & Lenzo, N. Renal outcomes of radioligand therapy: Experience of 177lutetium-prostate-specific membrane antigen ligand therapy in metastatic castrate-resistant prostate cancer. *Clin. Kidney J.* **13**(6), 1049–1055 (2021).
32. Scheinberg, A. D. & McDevitt, R. M. Actinium-225 in targeted alpha-particle therapeutic applications. *Curr. Radiopharm.* **4**(4), 306–320 (2012).
33. Kratochwil, C. *et al.* PMPA for nephroprotection in PSMA-targeted radionuclide therapy of prostate cancer. *J. Nucl. Med.* **56**(2), 293–298 (2015).
34. Gaertner, F. C. *et al.* Uptake of PSMA-ligands in normal tissues is dependent on tumor load in patients with prostate cancer. *Oncotarget* **8**(33), 55094–55103 (2017).
35. Langbein, T. *et al.* The influence of specific activity on the biodistribution of ^{18}F-rhPSMA-7.3: A retrospective analysis of clinical positron emission tomography data. *J. Nucl. Med.* https://doi.org/10.2967/jnumed.121.262471 (2021).

Acknowledgements
The authors would like to thank the cyclotron team of the department nuclear medicine of Ghent University Hospital for the production of the radiotracer and the outstanding cooperation.

Author contributions
S.P., J.V., K.K. and F.D.V. contributed to the study concept and study design, data was collected by S.P., J.V., E.D.C., B.D., K.K., L.P. and C.V. The manuscript was writing by S.P. All authors revised and approved the final manuscript.

Funding
The study was supported by the Flemish foundation FWO TBM (T001517).

Competing interests
The authors declare no competing interests.

Additional information
Supplementary Information The online version contains supplementary material available at https://doi.org/10.1038/s41598-021-02104-6.

Correspondence and requests for materials should be addressed to S.P.

Reprints and permissions information is available at www.nature.com/reprints.

Publisher's note Springer Nature remains neutral with regard to jurisdictional claims in published maps and institutional affiliations.